Available online at www.sciencedirect.com
ScienceDirect
Catalysis Today 133–135 (2008) 367–373
CATALYSIS TODAY
www.elsevier.com/locate/cattod

Preparation and characterization of nickel-based mixed-oxides and their performance for catalytic methane decomposition

M.E. Rivas [a], J.L.G. Fierro [a,*], R. Guil-López [a], M.A. Peña [a], V. La Parola [a], M.R. Goldwasser [b,*]

[a] Instituto de Catálisis y Petroleoquímica, CSIC, Cantoblanco, 28049 Madrid, Spain
[b] Centro de Catálisis Petróleo y Petroquímica, Escuela de Química, Facultad de Ciencias, Universidad Central de Venezuela, Apartado 40600, Los Chaguaramos, Caracas 1020-A, Venezuela

Available online 31 January 2008

Abstract

The preparation of three different types of mixed nickel oxides is described. These systems include: (i) the perovskite $LaNiO_3$ oxide, (ii) a mixed-oxide derived from a hydrotalcite Ni–Al (64:38) precursor, and (iii) the spinel-type $NiAl_2O_4$ oxide. These systems were prepared with the aim of studying the activation procedure that develops small nickel nanoparticles deposited on a La_2O_3 or Al_2O_3 substrate active in H_2 production through catalytic decomposition of CH_4. Different preparation procedures have been applied to each precursors (i)–(iii). Perovskite-type oxide $LaNiO_3$ was prepared by the sol–gel methodology (citrates method). Mixed oxide derived from hydrotalcite was obtained by co-precipitation using urea as a basic agent. $NiAl_2O_4$ spinel synthesis was performed by the ceramic method. The three oxide-type materials were characterized by XRD, BET specific area, TPR and XPS. Characterization results showed that the preparation methods used allow formation of highly crystalline and homogeneous oxide precursors. After activation, the oxide precursors showed a high activity in the decomposition reaction of CH_4. The catalysts derived from hydrotalcite mixed oxide showed the highest activity with CH_4 conversions reaching 50% at 500 °C.

Keywords: Nickel catalysts; NiAl hydrotalcite precursors; Methane decomposition; TPR; XRD and XPS characterization

1. Introduction

Methane, as the principal component of natural gas, is an ideal source for hydrogen production due to its enormous proven reserves and also to the high H/C atomic ratio in CH_4 molecule (H/C ratio in methane is 4). Among the routes outlined to obtain hydrogen from CH_4, the catalytic decomposition of methane remains prominent [1]. The CO-free hydrogen produced by CH_4 decomposition appears particularly suited for fuel cell applications since there is no need of further purification steps. The decomposition reaction is moderately endothermic and produces carbon as a by-product:

$$CH_4 \rightarrow C + 2H_2 \qquad \Delta H = 45.0\,\mathrm{kJ/mol}. \tag{1}$$

Indeed, this reaction is much less endothermic than the methane steam reforming, (MSR), which is the conventional technology employed in the industry for the massive production of hydrogen:

$$CH_4 + H_2O \rightarrow CO + 3H_2 \qquad \Delta H = 225.9\,\mathrm{kJ/mol}. \tag{2}$$

In the MSR reaction, methane conversions close to that predicted by the thermodynamic equilibrium can be obtained over Ni catalysts or supported catalysts (1), although important differences in CO and H_2 selectivity's are usually found for a few metal catalysts.

Reactions involved in the catalytic conversion of methane show two major drawbacks: (i) the temperature required to conduct reactions (1) and (2) at a reasonable rate is rather high, usually above 800 °C, which results detrimental for catalyst performance since sintering of metal particles occurs simultaneously with subsequent activity lose; (ii) carbon deposits are developed along the reaction on the surface of metal particles which block the metal sites responsible for the reaction. For this reason, the development of active and thermally and chemically stable catalyst systems is of prime importance.

* Corresponding authors.
E-mail addresses: jlgfierro@icp.csic.es (J.L.G. Fierro), mgoldwas@reacciun.ve (M.R. Goldwasser).

0920-5861/$ – see front matter © 2007 Elsevier B.V. All rights reserved.
doi:10.1016/j.cattod.2007.12.045

Many studies have been carried out to prepare mixed-oxides with perovskite structure [2–5] and mixed-oxides derived from hydrotalcite precursors [6] suited for methane conversion reactions such as steam reforming, partial oxidation and dry reforming. These mixed-oxides are highly stable under the severe conditions imposed by these reactions, i.e. high pressure, high temperature and presence of steam in the reaction medium. In addition, the efficient use of these catalyst precursors implies necessarily a high dispersion of metal phases which can be achieved by controlled segregation of the active phase. This objective can be reached by starting with a crystalline precursor, such as a mixed oxide perovskite type structure, or by decomposing an ordered lamellar structure such as the mixed-oxides derived from hydrotalcite.

Within this framework, the present work was undertaken to compare the catalytic performance of two different nickel-based metal oxides for the methane decomposition into CO-free hydrogen. One of this is the $LaNiO_3$ perovskite-type oxide and the other is a mixed oxide derived from an aluminium and nickel-containing hydrotalcite precursor.

2. Experimental

2.1. Preparation of catalyst precursors

The $LaNiO_3$ perovskite-type oxide was prepared according to the modified citrate method [7]. Stoichiometric amounts of $La(NO_3)_3{\cdot}xH_2O$ (Merck, reagent grade) and of $Ni(NO_3)_3{\cdot}6H_2O$ (Merck, reagent grade) were dissolved in distilled water and then added to a second solution containing equimolecular amounts of citric (99.5, Riedel-de Haën) and ethylene glycol (99.5%, Riedel-de Haën) as a polydentate ligand. The excess of water was slowly removed in a rotary-evaporator until a viscous liquid was obtained. Subsequently, this viscous material was slowly heated in air atmosphere at a rate of 1 °C/min from room temperature to 800 °C and maintained at this temperature for 5 h. These conditions are essential to obtain a crystalline material.

The nickel and aluminium mixed oxide was prepared from an Al–Ni-containing hydrotalcite (Ni–Al-HT), with 1.8 Ni/Al atomic ratios. The hydrotalcite precursor was prepared by co-precipitation [8], using urea (Merck, reagent grade) as precipitating agent. Urea-salts concentration was: urea/$[Al^{3+} + Ni^{2+}]$ = 3/1 and salt precursors used were $NiCl_2{\cdot}6H_2O$ $6H_2O$ and $AlCl_3{\cdot}6H_2O$ (Panreac, 95%). The methodology included adding urea solution over another solution containing Al^{3+} and Ni^{2+} salts. The precipitate was maintained at 95 °C under vigorous stirring. The solid was separated by filtration and washed repeatedly with distilled water, dried at 100 °C and finally calcined at 800 °C for 4 h in air. Under these conditions, an Al–Ni-mixed oxide was obtained, hereafter referred as MO-HT-800.

A reference $NiAl_2O_4$ spinel material was synthesized by ceramic methodology. For this purpose, $NiCl_2{\cdot}6H_2O$ (Panreac 98%) and $AlCl_3{\cdot}6H_2O$ (Panreac 95%) were mixed in an agate mortar and calcined at 1000 °C for 10 h. After calcining, the solid was grounded and calcined again at the same temperature for 2 h.

2.2. Characterization of catalyst precursors

Oxide catalysts precursors were characterized by different techniques, including X-ray diffraction (DRX), specific surface area (BET), temperature-programmed reduction and photo-electron spectroscopy (XPS).

X-ray powder diffraction (XRD) patterns of all calcined samples were obtained with nickel-filtered Cu Kα radiation (λ = 1.538 Å) using a Seifert 3000P instrument. XRD diffractograms were collected in the 2θ range 5–80°, in steps of 2°/min. Phase identification was carried out by comparison with the JCPDF database cards. Particle size of nickel crystallites were determined by means of the Scherrer equation using the Ni (1 1 1) reflection at $2\theta = 44.5°$ for line broadening measurements. Specific surface areas were calculated using the BET method from the nitrogen adsorption isotherms, recorded at the temperature of liquid nitrogen on a Micromeritics ASAP 2100 apparatus, taking a value of 0.162 m^2 for the cross-sectional area of the N_2 molecule adsorbed. Prior to the adsorption measurements, samples were outgassed at 150 °C.

Temperature-programmed reduction (TPR) experiments were performed on a semiautomatic Micromeritics TPD/TPR 2900 apparatus interfaced with a microcomputer. Samples of about 30 mg were placed in a U-shape quartz tube first purged in a synthetic air stream at 200 °C for 1 h and then cooled to room temperature. Reduction profiles were recorded passing a 10% H_2/Ar flow at a rate of 50 mL/min while heating at a rate of 10 °C/min from room to 950 °C. A cold-trap was placed just before the TCD of the instrument to remove the water from the exit stream.

Surface analysis were carried out on a VG ESCAALAB 200R electron spectrometer provided with Al Kα ($h\nu$ = 1486.6 eV, 1 eV = 1.6302×10^{-19} J) X-ray source and a hemi-spherical electron analyzer. The powder samples pressed in 8 mm diameter copper troughs were fixed on the *XYZ* manipulator. The base pressure in the analysis chamber was maintained below 4×10^{-9} mbar during data acquisition. Energy of the analyzer was set at 50 eV, for which the resolution as measured by the full width at half maximum (FWHM) of the $Au4f_{7/2}$ core level was 1.7 eV. The binding energies were referenced to the C1s peak at 284.6 eV due to adventitious carbon. Data processing was performed with the *XPS peak* program, the spectra were decomposed with the least squares fitting routine provided by Gaussian/Lorentzian (90/10) software with product function and after subtracting a Shirley background, Atomic fractions were calculated using peak areas normalized on the basis of sensitivity factors.

2.3. Catalytic activity

Activity measurements were performed in a continuous flow fixed-bed catalytic reactor at atmospheric pressure. Sixty milligrams catalyst was placed between quartz glass plugs in the centre of a cylindrical tube reactor (4 mm i.d. placed within another one of 6 mm i.d.). The temperatures at the internal and external walls of the catalyst reactor were measured by Ni–Cr thermocouples.

Prior to activity measurements, catalyst precursors were reduced in a 10% H_2/N_2 mixture at 750 °C for 1.5 h to generate the Ni^0 metal phase. Subsequently, the reactor was flushed in a nitrogen stream while cooling to room temperature. The reaction was carried out by feeding a 7% CH_4/N_2 at a WHSV = 146 L/h g and scanning reaction temperatures in the 25–850 °C range. Reaction products were analyzed on-line by a Varian 3400 gas-chromatograph provided with thermal conductivity detector and columns packed with Porapak N and 13X molecular sieves. Estimated error of gas-phase composition was within 5%.

3. Result and discussion

3.1. X-ray diffraction analysis

X-ray diffraction profiles of $LaNiO_3$, Al–Ni hydrotalcite and $NiAl_2O_4$ oxide precursors are displayed in Fig. 1. La–Ni perovskite-type oxide exhibits all diffraction lines of a dominant rhombohedra $LaNiO_3$ structure (JCPDS-ICDD 10-341). In addition, very weak lines indexed to a NiO phase were detected, indicating that a small amount of nickel was not incorporated to the $LaNiO_3$ phase. Similarly, the diffraction profile of Ni–Al hydrotalcite belongs to the takovite single phase (JCPDS-ICDD 15–87) with a high crystallization degree. The diffraction pattern of $NiAl_2O_4$ spinel shows only diffraction lines of this structure (JCPDS-ICDD 78-0552) with high crystallinity.

Fig. 2 displays the X-ray diffraction pattern of the mixed oxide produced upon thermal decomposition of the hydrotalcite precursor. This pattern shows diffraction lines of a mixture of nickel and aluminium oxides together with that of $NiAl_2O_4$ spinel.

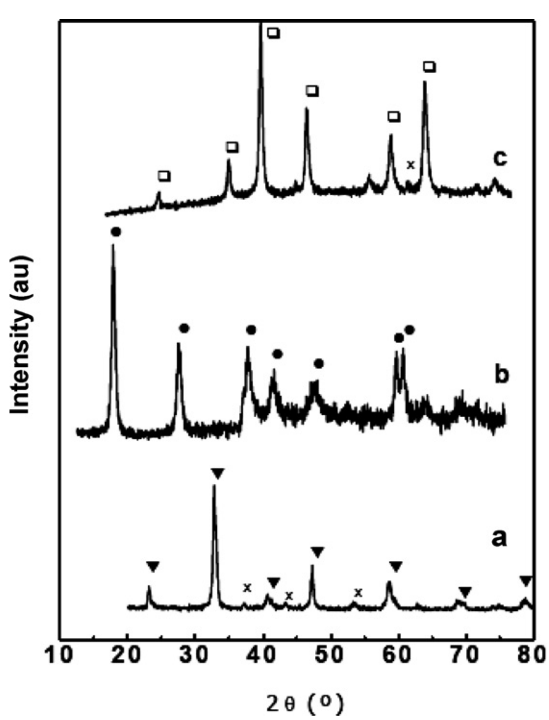

Fig. 1. X-ray diffraction profiles of nickel compounds: (a) $LaNiO_3$; (b) hydrotalcite Ni–Al; (c) $NiAl_2O_4$. (▼) $LaNiO_3$; (●) takovite; (□) $NiAl_2O_4$; (×) NiO.

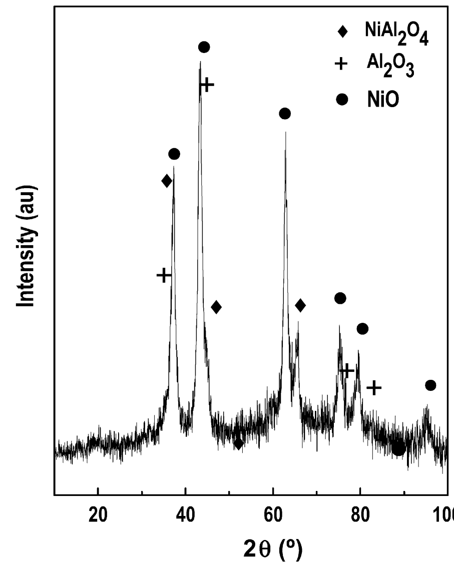

Fig. 2. X-ray diffraction profiles of Al–Ni-mixed–oxide derived from the hydrotalcite precursor (OM-HT-800).

Diffraction profiles of the H_2-reduced and after-reaction samples are shown in Figs. 3 and 4, respectively. Reduction and testing to measure catalytic activity of the samples were performed at the same conditions (750 °C for 1.5 h).

After reduction of precursor oxides, $LaNiO_3$, OM-HT-800, production of highly dispersed Ni^0 particles on the surface of an oxide substrate is expected. Results show that the crystalline structure of $LaNiO_3$ perovskite-type phase decomposed to Ni^0 crystallites with particle size of about 25 nm dispersed on La_2O_3 surface. Similarly, reduction of Ni–Al hydrotalcite precursor produces metallic Ni^0 particles, with average particle size of 22 nm, on the surface of Al_2O_3. However, a small fraction of unreduced nickel remains in a $NiAl_2O_4$ phase. Finally, the XRD pattern of the $NiAl_2O_4$ spinel indicates that only a fraction of Ni^{2+} cations of this structure are reduced, with crystallite sizes of ca. 12 nm, while most of the $NiAl_2O_4$ spinel remains unreduced in accordance with TPR profiles shown in Fig. 5.

X-ray diffraction profiles of after-reaction catalysts (Fig. 4) reveal the formation of Ni^0 crystallites. Calculation of Ni^0 mean crystallite size on these after-reaction catalysts showed that an increase of the particle size occurs as a consequence of sintering of metal particles. Such increase is clearer for $NiAl_2O_4$ where crystallites size changes from 12 nm for the as-synthesized to 24 nm for the after-reaction samples, showing that Ni^0 crystallites are less stable in $NiAl_2O_4$. On the contrary, the Ni^0 crystallite size increase is much less marked for after-reaction OM-Ni–Al (from 22 to 27 nm) and $LaNiO_3$ (from 25 to 29 nm) samples. It is important to note that the diffraction profiles of after-reaction OM-HT-800 and $NiAl_2O_4$ samples exhibit an intense line at $2\theta = 26^\circ$ which corresponds to graphitic carbon deposited on the catalyst surface during the reaction.

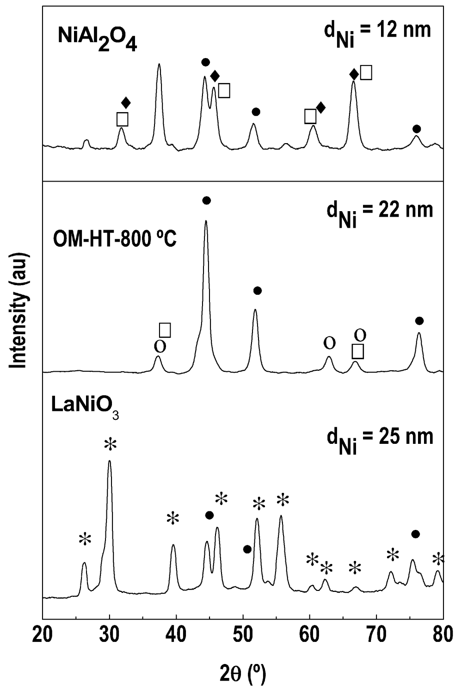

Fig. 3. X-ray diffraction profiles of H_2-reduced oxide precursors. (●) Ni^0; (★) La_2O_3; (□) $NiAl_2O_4$; (○) Al_2O_3 (1–1303); (◆) Al_2O_3 (80–1385).

3.2. Precursors BET specific surface area

Table 1 compiles BET specific surface area (BET) of calcined precursors. The perovskite-type oxide ($LaNiO_3$), prepared by the sol–gel method shows a BET specific surface area of 7 m^2/g. This value is somewhat higher than that obtained by other preparation methods such as solid-state reaction and co-precipitation from aqueous solutions of La^{3+} and Ni^{2+} salts. In agreement with a previous work [9], the specific surface area of metal oxides with perovskite structure, subjected to calcination at high temperatures, correspond mainly to particles approaching a spherical geometry, which is characteristic of non-porous materials.

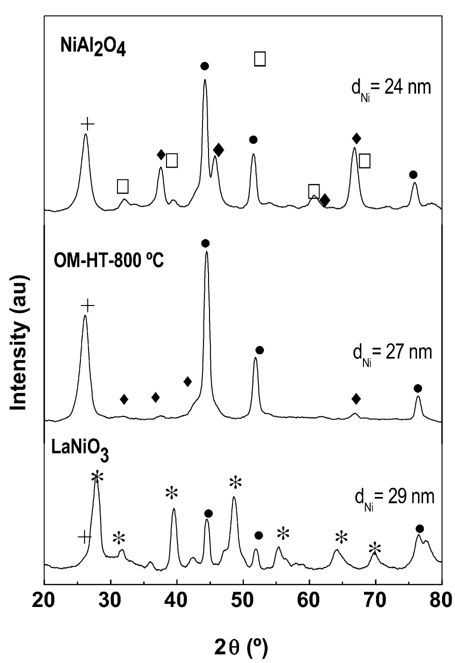

Fig. 4. X-ray diffraction profiles of the catalysts after on-stream operation. (●) Ni^0; (★) La_2O_3; (□) $NiAl_2O_4$; (+) graphite.

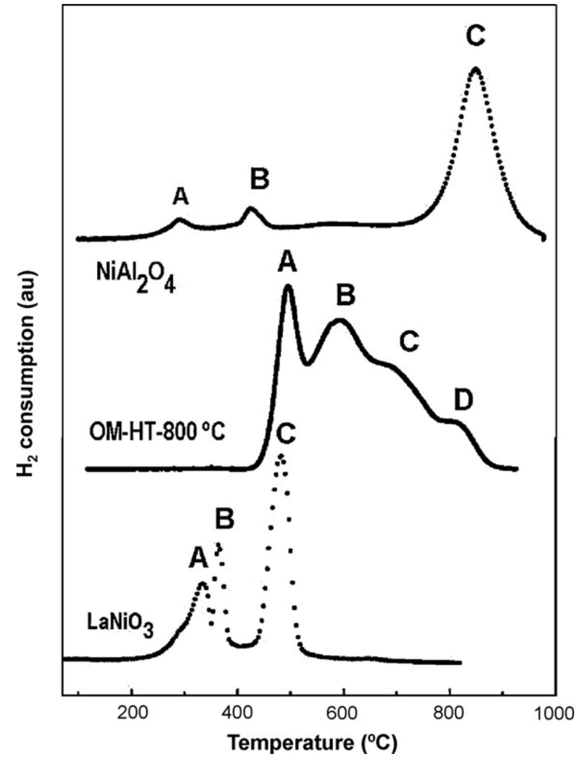

Fig. 5. Temperature-programmed reduction profiles of oxide precursors: $LaNiO_3$, OM-HT-800 and $NiAl_2O_4$.

Mixed oxide generated by calcining Al–Ni hydrotalcite at 800 °C displays a rather high BET specific surface area (83 m^2/g) as it would be expected from a mesoporous material. In addition, the $NiAl_2O_4$ spinel used as a reference shows a relatively high BET specific surface area (33 m^2/g), even though it was prepared by the ceramic method and calcined 1000 °C. This value contrasts with BET surface area values of samples prepared by conventional precipitation and complex-forming methods.

3.3. Temperature-programmed reduction (TPR)

Temperature-programmed reduction profiles of the precursor oxides are displayed in Fig. 5. The $LaNiO_3$ perovskite-type profile calcined at 900 °C shows peaks typical of reduction of the perovskite-type phase [9]. Quantitative data of hydrogen-consumption indicate that a small fraction of nickel should be

Table 1
BET specific surface areas (m^2/g) of precursor oxides

Calcination temperature	800 °C	1000 °C
$LaNiO_3$	7	–
OM-Ni–Al	83	–
$NiAl_2O_4$	–	33

segregated as a separate NiO phase. This result is consistent with X-ray diffraction profiles where lines of a minor NiO phase accompanying those of a major $LaNiO_3$ phase were observed. The reduction process proceeds in three steps: a first one taking place within the 250–350 °C range attributed to the reduction of the minor NiO phase (labelled A) segregated on the surface of $LaNiO_3$. The second reduction peak (labelled B) corresponds to the reduction of Ni^{3+} ions of $LaNiO_3$ perovskite into an intermediate brownmillerite-type $La_2Ni_2O_5$ structure in which nickel is present as Ni^{2+} ions ($LaNiO_3 \rightarrow La_2Ni_2O_5$). The third peak (marked as C) is placed around 450 °C and corresponds to the reduction of Ni^{2+} ions in the brownmillerite to metallic Ni^0. Thus, upon reduction of the $LaNiO_3$ at temperatures above 500 °C, metal Ni^0 particles are generated and remain dispersed on the lanthanum phase (Ni^0/La_2O_3), which is the active phase in the methane decomposition reaction.

The reduction profile of the Al–Ni hydrotalcite precursor calcined at 800 °C (OM-HT-800) also displays four H_2-consumption peaks, attributed to nickel reduction phases with different morphology and degree of interaction with the supports, as reflected in the diffraction profile of this precursor (Fig. 5). The first H_2-consumption peak at around 420 °C is assigned to reduction of dispersed and well-crystallized NiO particles (labelled A). The second reduction within the temperature range 500–700 °C corresponds to reduction of NiO particles strongly interacting with the Al_2O_3 substrate (labelled B and C) [10]. Finally, the reduction peak at temperatures about 800 °C is attributed to reduction of Ni^{2+} ions incorporated into the major $NiAl_2O_4$ spinel phase (labelled D). The maximum H_2-consumption peak placed around 850 °C is assigned to reduction of $NiAl_2O_4$ phase into metallic Ni^0. In addition, a small reduction peak placed around 245 °C is associated to reduction of a very small fraction of nickel present as a separate NiO phase and deposited on the $NiAl_2O_4$ surface. Similarly, another very weak H_2-consumption peak appears around 390 °C, which is also associated to NiO particles of smaller size and/or interacting more strongly with the major $NiAl_2O_4$ substrate.

3.4. Photoelectron spectroscopy (XPS)

XPS spectra of the Ni 2p core-level were recorded for the three oxide precursors ($LaNiO_3$, OM-HT-800 and $NiAl_2O_4$) to determine both chemical state of nickel and surface concentration of the elements.

Fig. 6 displays XPS spectra of Ni 2p core-levels of calcined samples and Table 2 compiles the binding energies (eV) of $Ni2p_{3/2}$, O1s and $La3d_{5/2}$ or Al2p core-levels. There is a strong overlapping in the spectrum of Ni 2p and La 3d levels in $LaNiO_3$ sample not observed in OM-HT-800 and $NiAl_2O_4$ samples. However, quantification is possible since the less intense Ni $2p_{1/2}$ level of the Ni 2p doublet appears sufficiently separated from the most intense Ni $2p_{3/2}$ one, which is strongly overlapped with the $La3d_{3/2}$ component. There is a good fitting of binding energies of $Ni2p_{3/2}$ level (855.3 eV) and $La3d_{5/2}$ (834.8 eV) in $LaNiO_3$ sample (Table 2) with the values previously reported for these perovskites (1–4).

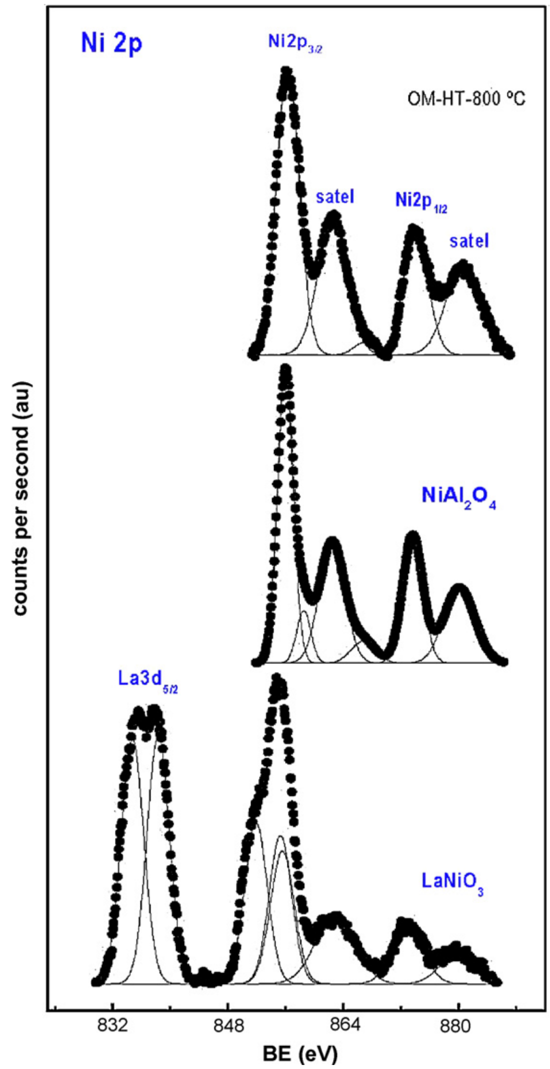

Fig. 6. Phoelectron spectra of the Ni2p core-level of oxide precursors: $LaNiO_3$, OM-HT-800 and $NiAl_2O_4$.

The BE's values of Ni $2p_{3/2}$ level of Ni^{2+} ions in OM-HT-800 and $NiAl_2O_4$ samples are higher (856.1–856.2 eV) showing that Ni^{2+} ions are mainly coordinated to oxide ions in a tetrahedral environment. However, it is inferred that a minor proportion of NiO species should also be present since the intensity ratio between each satellite line (the fingerprint of Ni^{2+} ions) and the main line is lower than expected for a $NiAl_2O_4$ spinel with 100% of Ni^{2+} ions in a tetrahedral environments of oxide ions.

It is interesting to note the presence of three O1s components characteristic of perovskite structures (1, 4). The first component at 529.0 eV is usually assigned to unsaturated O^{2-} ions on the perovskite surface. The second component at 530.6 eV corresponds to Ni–O–La bonds, and the third one located at 531.9 eV comes from surface CO_3^{2-} and/or hydroxyl groups developed on the exposed La^{3+} ions. Another important observation to be considered in the XPS analysis is the difference in the Ni/Al atomic ratio in the $NiAl_2O_4$ sample. The experimental value of the Ni/Al ratio for this sample is 0.073, much lower than 0.500 expected from the nominal composition

Table 2
Binding energies (eV) of core-levels of precursor oxides

	Ni $2p_{3/2}$	O 1s	$La3d_{5/2}$	Ni/Al at	Ni/La at
$NiAl_2O_4$	856.1	531.3	–	0.073	–
OMNiAl	856.2	529.9, 531.7	–	0.589	–
$LaNiO_3$	855.3	529.0, 530.6, 531.9	834.8	–	1.13

of Ni/Al ratio in pure $NiAl_2O_4$. This result indicates, undoubtedly, that a certain fraction of nickel exists in a separate phase, no detected by X-ray diffraction, probably because it is in an amorphous structure deposited on the surface of the $NiAl_2O_4$ spinel, which determines a very low surface exposure in this sample. On the contrary, the $LaNiO_3$ sample shows a surface ratio Ni/La = 1.13, which is close to the nominal Ni/La = 1.00 atomic ratio in pure $LaNiO_3$.

3.5. Catalytic activity

Prior to catalytic measurements, the $LaNiO_3$, OM-HT-800 and $NiAl_2O_4$ precursors were reduced within the reactor at 750 °C for 1.5 h. After cooling to room temperature, a flow of 7% CH_4/N_2 mixture was introduced and activity behaviour was examined by increasing temperature from room to 850 °C. The performance of nickel catalysts was found to be quite different. CH_4 conversion profiles as a function of reaction temperature are shown in Fig. 7. At temperatures higher than 400 °C, the three Ni catalysts were active in the methane decomposition reaction.

The catalyst derived from OM-HT-800 precursor was the most active in the reaction since CH_4 conversion starts at temperature around 410 °C. The one derived from $NiAl_2O_4$ spinel is also quite active though reaction starts at temperature somewhat above, near 450 °C. The less active catalyst was that obtained from $LaNiO_3$ oxide-type perovskite, activity was observed only at temperatures above 550 °C. All catalysts reached almost complete CH_4 conversion at reaction temperatures close to 750 °C, though their stability was quite different. Particularly, the catalyst derived from the $NiAl_2O_4$ precursor deactivated rapidly with activity dropping to ca. 20% at of 800 °C.

One of the reasons of the better catalytic performance observed with the activated OM-HT-800 catalyst is its much higher specific surface area, which may yield in parallel a high dispersion of Ni^0 crystallites on the catalyst surface upon activation with the subsequent improvement in catalyst performance. The relatively good stability of this catalyst can be due to interaction of Ni^0 particles generated along the activation process with alumina surface which may inhibit the sintering of metal particles. On the contrary, the catalyst derived from the $NiAl_2O_4$ spinel shows only a very small fraction of reduced nickel (Ni^0) (cf. Fig. 5) at rather low temperatures. This fraction comes from the reduction of the minor separate NiO phase of the oxide precursor. Moreover, the diffraction profiles of this catalyst used in reaction indicate that the Ni^0 particles became markedly sinterized along the course of the reaction (Figs. 3 and 4). This would explain the drastic drop of CH_4

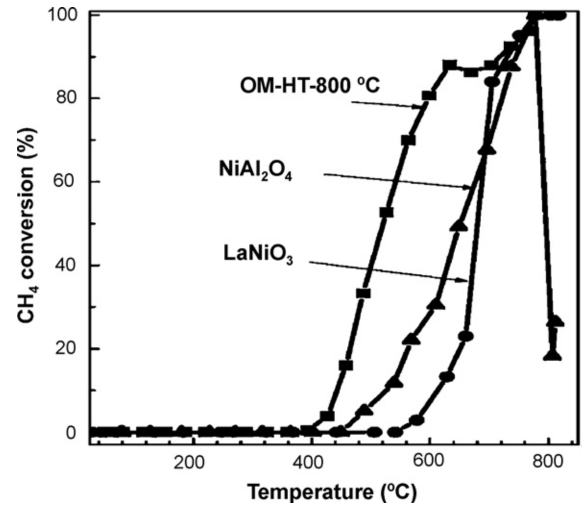

Fig. 7. CH_4 conversion as a function of temperature for catalysts derived from $LaNiO_3$, OM-HT-800 and $NiAl_2O_4$ precursors.

conversion once the catalyst has been severely sinterized (Fig. 7), due to the fact that aggregated Ni^0 particles facilitate the formation of coke residues which encapsulate or cover metallic Ni particles, and hence the catalyst became deactivated [11,12].

Concerning the catalyst stability, the system derived from the $LaNiO_3$ precursor displays an exceptional behaviour. This system shows complete and maintained CH_4 conversion at temperatures above 750 °C. As it has been previously documented (1, 2), one of the properties of the metallic particles generated during the reduction of cation at position B in the perovskite structure (Ni^{3+} in this case) is that surface and bulk diffusion of nickel atoms once generated is inhibited as a consequence of the physical barriers established by the La_2O_3 particles simultaneously produced along the reduction of $LaNiO_3$ crystallite precursor. Therefore, the metallic Ni^0 crystallites maintain a good dispersion on the La_2O_3 surface still keeping a low BET specific surface area. On the basis of this argument, it can be concluded that the good stability of the catalyst derived upon activation of $LaNiO_3$ precursor is mainly due to the ability to stabilize the Ni^0 crystallites in a high dispersion degree on a La_2O_3 matrix, thus limiting the extent of sintering of metallic particles.

4. Conclusions

(1) X-ray diffraction and temperature-programmed reduction reveal that the methodologies of preparation of catalyst precursors result in highly crystalline and homogeneous oxide structures.
(2) The type of nickel precursor influences to a large extent the catalytic performance for methane decomposition reaction. Catalyst prepared from mixed oxide derived from hydrotalcite precursor is the most active in the target reaction. This behaviour is mainly due to the high specific area of the oxide precursor.
(3) The most stable catalyst is the one derived from the $LaNiO_3$ perovskite. This catalyst maintains complete conversion

levels at temperatures above 750 °C. The stability of the $LaNiO_3$ catalyst is determined by the formation of highly dispersed nickel crystallites, obtained upon H_2-reduction, in close contact with the La_2O_3 substrate.

Acknowledgments

MER gratefully acknowledges financial support for a doctoral fellowship (I3P-program) from the European Social Fund. Authors also acknowledge financial support from MEC, Spain (Project ENE2004-07345-C03-01/ALT).

References

[1] M.A. Peña, J.P. Gomez, J.L.G. Fierro, Appl. Catal. A: Gen. 144 (1996) 7, and references therein see, for instance.
[2] L.G. Tejuca, J.L.G. Fierro, J.M.D. Tascon, Adv. Catal. 36 (1989) 385.
[3] M.A. Peña, J.L.G. Fierro, Chem. Rev. 101 (2001) 1981.
[4] M.R. Goldwasser, M.E. Rivas, E. Pietri, M.J. Pérez-Zurita, M.L. Cubeiro, A. Griboval-Constant, G. Leclercq, J. Mol. Catal. A: Gen. 228 (2005) 325.
[5] S. Ponce, M.A. Peña, J.L.G. Fierro, Appl. Catal. B: Environ. 24 (2000) 193–205.
[6] K. Takeira, T. Shisido, P. Wang, T. Kosaka, K. Takaki, J. Catal. 221 (2004) 43–54.
[7] M.P. Pechini, US Patent 3,330,673, 1967.
[8] F. Cavani, F. Trifinò, A. Vaccari, Catal. Today 11 (2) (1991) 173.
[9] L. Bedel, A.C. Roger, C. Estournès, A. Kinnemann, Catal. Today 85 (2–4) (2003) 207.
[10] H. Provendier, C. Petit, C. Etournès, S. Libs, A. Kinnemann, Appl. Catal. A: Gen. 180 (1999) 163.
[11] G. Li, L. Hu, C. Estournès, J.M. Hill, Appl. Catal. A: Gen. 301 (2006) 16–24.
[12] J.I. Villacampa, C. Royo, E. Romeo, J.A. Montoya, Appl. Catal. A: Gen. 252 (2003) 363.